This article has been accepted for publication in a future issue of this journal, but has not been fully edited. Content may change prior to final publication. Citation information: DOI 10.1109/TMAG.2016.2525007, IEEE Transactions on Magnetics

Equivalent Circuit Modeling of a Hysteresis Interior Permanent Magnet Motor for Electric Submersible Pumps

S. F. Rabbi, *Student Member, IEEE,* and M. A. Rahman, *Life Fellow, IEEE*

Department of Electrical & Computer Engineering, Memorial University of Newfoundland, St. John's, NL A1B 3X5, Canada

This paper presents the magnetic and electrical equivalent circuits of a hysteresis interior permanent magnet (IPM) motor. A hysteresis IPM motor is a solid rotor hybrid synchronous motor combining hysteresis phenomena and permanent excitation in the rotor. When installed in thousands of feet under the sea to drive an electric submersible pump (ESP), it can self-start the ESP without the need of any position sensors, and can improve the efficiency, the performance and the reliability of the ESP. In this paper, equivalent circuit models are used to predict the transient run-up responses of a 2.5kW prototype hysteresis IPM motor. Analysis results are compared with 2-D finite element analysis (FEA) results as well as experimental results. There exists a reasonably close agreement between analytical, FEA and experimental results which validates the accuracy of the equivalent circuit models of a hysteresis IPM motor.

Index Terms— **Equivalent circuits, permanent magnet motors, magnetic hysteresis, modeling.**

I. Introduction

An electric submersible pump (ESP) is a motor/pump configuration made up of multi-stage centrifugal pumps driven by electric 3 phase ac submersible motors. ESPs are widely used as downhole artificial lift devices in both offshore and onshore oil fields for producing up to 40000 barrels of fluid per day at various depths from 1000 to over 12000 feet [1]. Bottomhole submersible motors are specially designed to withstand high temperature, high mechanical and electrical stress and high inrush current. Polyphase squirrel-cage rotor sealed submersible induction motor (IM) drives have traditionally been used in ESPs [1-2]. However, IM driven ESPs suffer from poor power quality, poor thermal stability and poor efficiency due to slip power losses in the rotor and also due to non-sinusoidal voltage and current waveforms [2]. It also experiences frequent failure and shaft breakdowns due to vibrations caused by extreme mechanical stress, especially during start-up of the pump. Thus, IM driven ESPs have poor reliability and relatively short run-life.

A hysteresis IPM motor is a hybrid synchronous motor that starts as a hysteresis motor and becomes an IPM motor at steady state. It has a high starting torque and moderate starting currents similar to a standard hysteresis motor. A hysteresis IPM motor drive does not need position sensors, has self-starting capability, wide operating range, good efficiency and high reliability. These are critical requirements of a submersible motor drive for ESPs. Thus, the hysteresis IPM motor ESP drive has the potential to replace the induction motor driven standard ESPs.

In the analysis of hysteresis IPM motors, modeling of hysteresis loops has been an issue of interest among the researchers [3-7]. There are several ways to model the hysteresis phenomenon of a magnetic material. Classical Preisach model, Jiles-Atherton model (JAM) and Hauser Energetic Model (HEM) are the most popular ones among them [3]. However, development of equivalent circuits for hysteresis IPM motors using these models is complicated. Another way is to approximate the shape of a hysteresis loop by using either parallelogram model or elliptical model [4-7]. Rahman and Qin have presented equivalent circuit modeling of hysteresis permanent magnet motors using parallelogram/rectangular modeling of the hysteresis loop [6]. Elliptical modeling is a better way for approximating hysteresis loops, and is more accurate and computationally simpler than the parallelogram/rectangular models [7]. In this paper, equivalent circuits of a hysteresis IPM motor are presented using the elliptical approximation of the hysteresis loop. Electrical and magnetic equivalent circuits in *d-q* axes have been illustrated and explained in this paper. Analytical simulations using the developed electrical equivalent circuits and finite element analysis have been carried to obtain the transient responses of a 3-phase 4-pole 208V, 2.5 kW laboratory prototype hysteresis IPM motor. Simulation results as well as experimental test results of the prototype motor are presented and analyzed in this paper.

II. Modeling of Hysteresis IPM Motor

A. Hysteresis IPM Motor

A hysteresis IPM motor is a hybrid design combining the features of conventional hysteresis motors and interior permanent magnet motors. Figs. 1(a) and 1(b) illustrate the rotor of a prototype hysteresis IPM motor and the conceptual design of a hysteresis IPM submersible motor driven ESP, respectively. The stator of the hysteresis IPM motor has a 3-Φ sinusoidally distributed double-layer winding arrangement. The rotor has a solid ring made of 36% Cobalt-Steel alloy which is a semi-hard composite magnetic material with high degree of hysteresis energy per unit volume. Radially magnetized arc-shaped rare earth Nd-B-Fe magnets are buried inside the hysteresis ring, and the ring is supported by a non-magnetic aluminum sleeve.

B. Modeling of Hysteresis Loops

Fig. 2 shows the major hysteresis loop of a hysteresis ring made of 36% Cobalt-Steel alloy. Elliptical modeling is a way to approximate the shape of the hysteresis loops of a material.

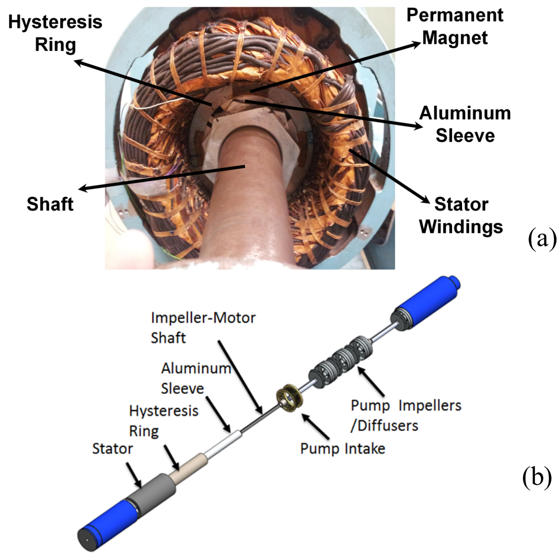

Fig. 1. A hysteresis IPM motor: (a) laboratory prototype and (b) ESP.

The flux density B and the magnetic field intensity H in an elliptical model can be expressed as follows [5-7],

$$B = B_m \cos(\omega t - \psi - \psi_0) \quad (1)$$

$$H = \left(\frac{B_m}{\mu}\right) cos(\omega t - \psi - \psi_0 + \delta) \quad (2)$$

$$\psi_0 = \tan^{-1} \frac{\frac{r_r \sin\delta}{p\mu}}{\frac{l_g p t_r}{\mu_0 r_g} + \frac{r_r}{p\mu}\cos\delta} \quad (3)$$

where B_m is the maximum flux density of the rotor material, μ is the permeability of the elliptic hysteresis loop, ω is the synchronous angular frequency, ψ ($\psi = p\theta_r$; θ_r is the mechanical angle of the rotor and p is the number of pole pairs) is the electrical angle coordinate in the stator frame, ψ_0 is the phase shift, r_g is the mean radius of the air-gap and δ is the hysteresis lag angle between B and H. More parameters are listed in the appendix.

C. Magnetic Equivalent Circuits

Figs. 3(a) and 3(b) present the d and q axis magnetic equivalent circuits of a hysteresis IPM motor. The permanent magnet is modeled as a mmf source $\mathcal{F}_{md}$ in series with a reluctance $\mathcal{R}_{md}$. Hysteresis effect is included in the circuit as a mmf source $\mathcal{F}_{hd}$. The d-q axis reluctances of the hysteresis material are modelled as nonlinear reluctances $\mathcal{R}_{hd}$ and $\mathcal{R}_{hq}$,

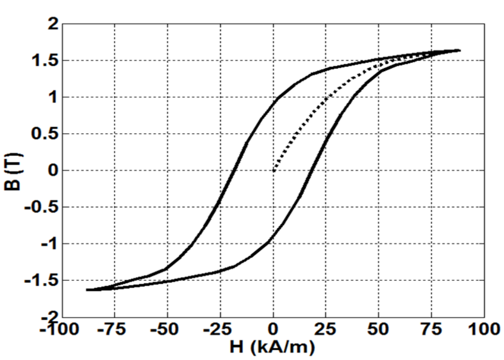

Fig. 2. B-H curves of 36% Cobalt-Steel alloy.

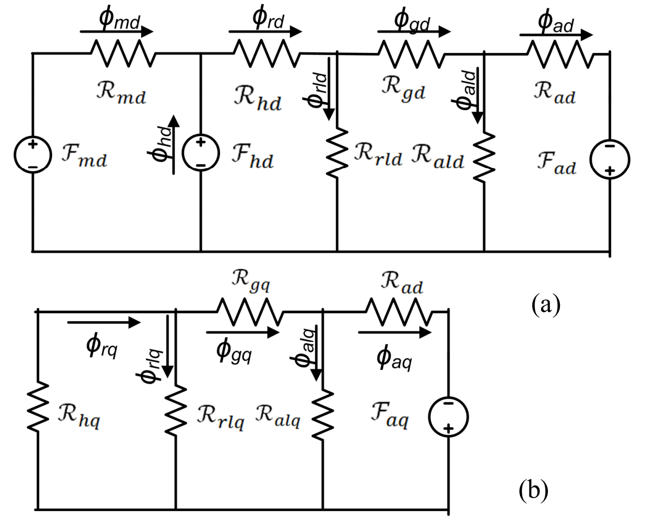

Fig. 3. Magnetic equivalent circuit: (a) d-axis and (b) q-axis.

respectively. $\mathcal{R}_{rld}$ and $\mathcal{R}_{rlq}$ are the d-q axis rotor leakage reluctances. The effects of hysteresis and permanent magnet mmfs are negligible in the q-axis, and are not included in the q-axis equivalent circuit. The d-q axis airgap reluctances are presented by $\mathcal{R}_{gd}$ and $\mathcal{R}_{gq}$, respectively. The primary armature magnetomotive forces in d-q axis are presented by $\mathcal{F}_{ad}$ and $\mathcal{F}_{aq}$, respectively. $\mathcal{R}_{ad}$ and $\mathcal{R}_{aq}$ are the d-q axis reluctances of the stator back-iron. The d-q axis total leakage reluctance of the stator are modelled by $\mathcal{R}_{ald}$ and $\mathcal{R}_{alq}$, respectively.

D. Electrical Equivalent Circuits

The d-q axis electrical equivalent circuits of a hysteresis IPM motor are depicted in Figs. 4(a) and 4(b). The permanent magnet is modeled as a constant current source I_m. Eddy current effect is included in the circuit by modeling it as an equivalent resistance R_e. Hysteresis effect is modeled as an equivalent hysteresis resistance R_h, and an equivalent hysteresis inductance L_{hr}. The analytical expression for the

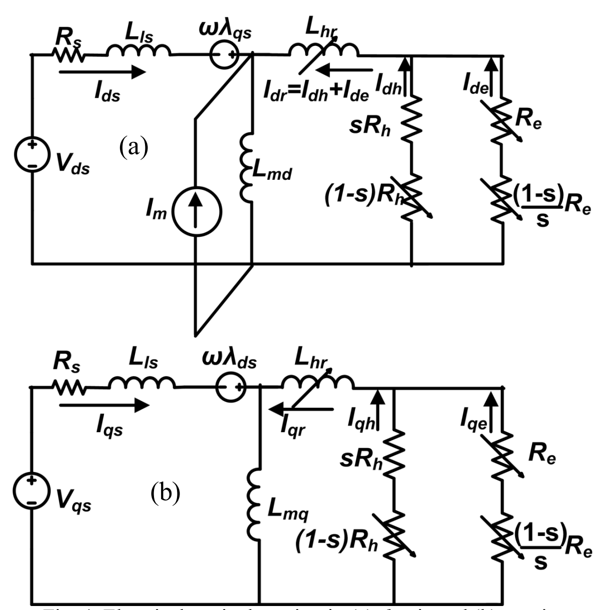

Fig. 4. Electrical equivalent circuit: (a) d-axis and (b) q-axis.

determining the hysteresis resistance R_h, the hysteresis inductance L_{hr} and the q-d axis airgap inductances L_{mq}, L_{md} are given by [5, 7],

$$R_{hr} = \omega_b \frac{3K_w^2 N_w^2 V_h \mu}{\pi^2 r_r^2} \sin\delta \tag{4}$$

$$L_{hr} = \frac{3K_w^2 N_w^2 V_h \mu}{\pi^2 r_r^2} \cos\delta \tag{5}$$

$$L_{mq} = k_{fq} L_m \,;\; L_{md} = k_{fd} L_m \tag{6}$$

$$L_m = \frac{6lK_w^2 N_w^2 \mu_0}{p^2 \pi^2 l_g} \tag{7}$$

The base angular frequency is denoted by ω_b, V_h is the volume of the hysteresis ring, K_w is the winding factor, N_w is the no. of series turns/phase, k_{fq} and k_{fd} are the form factors due to the saliency. The form factors are defined as [8],

$$k_{fq} = \frac{4}{\pi} \frac{\alpha}{1-\alpha^2} \cos\frac{\pi}{2}\alpha \tag{8}$$

$$k_{fd} = \frac{1}{\pi}(\alpha\pi - \sin\alpha\pi) \tag{9}$$

where α is equal to the ratio of the width of the pole shoe and to the pole pitch.

Hysteresis and eddy current resistances are divided into two components. One component reflects the hysteresis loss and the eddy current loss in the rotor, modeled by R_e and sR_h, respectively. The other component contributes to the output power of the motor, combining power derived from the effective eddy current resistance and the effective hysteresis resistance which are expressed as $((1-s)/s)R_e$ and $(1-s)R_h$, respectively, where s is the slip of the motor. At synchronous operation mode, the hysteresis effect is modeled as a current source, I_{hs} and can be expressed as,

$$I_{hs} = I_s \sin\delta \tag{10}$$

where I_s is the magnitude of the supply current.

III. Simulation Results

A 3-phase 4-pole 208V 2.5kW hysteresis IPM motor model is studied using finite element analysis and equivalent circuit solutions. Magnetic transient solver of ANSYS Maxwell software is used for finite element analysis of the motor. The core loss for 36% cobalt steel alloy is determined using advanced vector hysteresis modeling technique by ANSYS [9]. Fig. 5(a) depicts the flux density inside the motor during the transient state. The flux lines are shown in Fig. 5(b). The magnetic flux lines leave the air-gap radially. Due to the presence of the hysteresis ring, maximum flux lines bend inside the hysteresis ring and become circumferentially distributed. Some flux lines travel through the ring radially. As a result, the flux lines are more concentrated in the region where the fluxes are circumferentially distributed. This also results in a higher magnitude of magnetic flux density in that region. The air-gap back-emf due to the magnets at no load is illustrated in Fig 6.

The simulated speed and torque responses of the motor are shown in Figs. 7 and 8, respectively. The motor is run by a 3-phase Δ-connected 208V 60Hz balanced ac supply. The motor starts smoothly and goes through some speed overshoots and undershoots during the synchronization process. A 5 N.m. load torque is applied at 5s. The response of the motor for sudden change in load is zoomed in the pictures. There is a close agreement between analytical and finite element results. The electromagnetic torque is comprised of an average asynchronous torque and a pulsating torque. The average asynchronous torque combines the hysteresis torque, the eddy

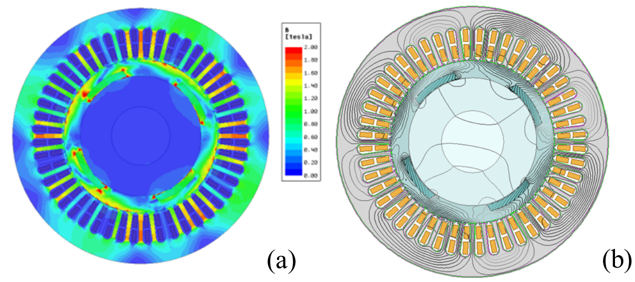

Fig. 5. Finite element analysis results: (a) flux density and (b) flux lines.

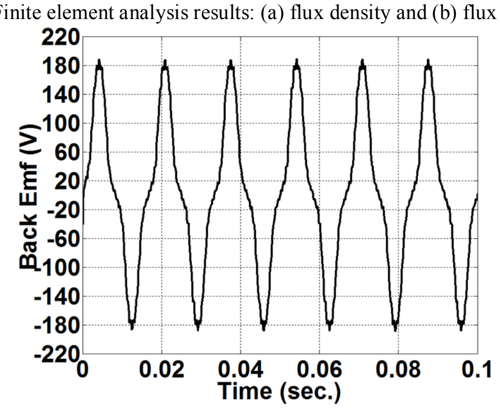

Fig. 6. Air-gap back-emf of the motor due to magnets.

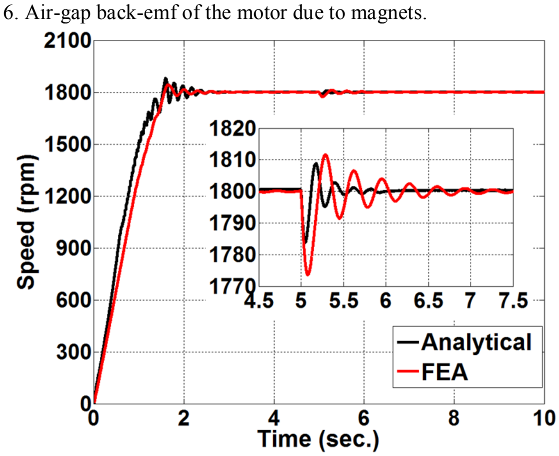

Fig.7. Analytical and FEA run-up responses of the motor.

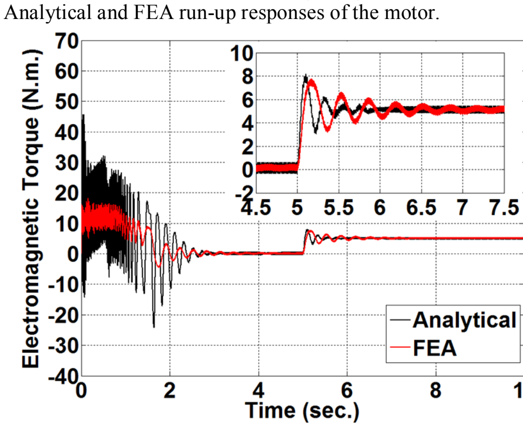

Fig. 8. Analytical and FEA torque responses of the motor.

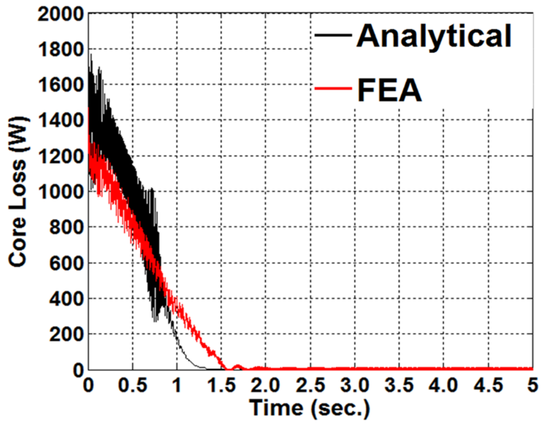

Fig. 9. Rotor core loss in the hysteresis ring.

current torque and the magnet brake torque. The pulsating torque assists the motor to a fast acceleration towards the synchronous speed. The torque pulsation is higher in the analytical result due to linearization of the state equations. Fig. 9 depicts the core loss in the hysteresis ring. The core loss is negligible at steady state as the eddy current loss becomes zero and the hysteresis ring behaves like magnets.

IV. EXPERIMENTAL RESULTS

A 4-pole 2.5kW laboratory prototype hysteresis IPM rotor has been built and tested in a 3-phase 4-pole 208V Mawdsley generalized machine. The motor is started from a fixed frequency 3-phase 208V 60Hz balanced ac supply. The motor was lightly loaded by a dc generator. Fig. 10 illustrates the analytical and experimental run-up responses of the motor. Load inertia and friction torque are included in the analytical model to match the conditions of the experimental set-up. The motor has a smooth start because of the high starting torque provided jointly by the hysteresis and eddy current torque. The motor synchronizes easily with small overshoots and undershoots. There are little oscillations in the experimental run-up response of the motor after synchronization due to mechanical vibrations. The starting current was clipped in the experimental results due to saturation effects of the current sensors. It is due to the laboratory limitation. As a result, comparative analysis between experimental and analytical

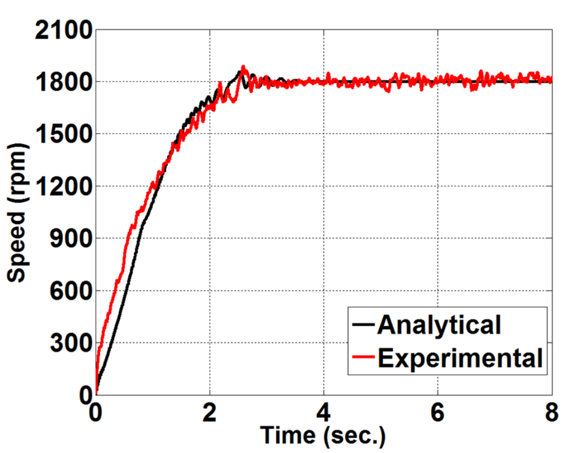

Fig. 10. Experimental and analytical run-up responses of the motor.

current transients could not be presented. The magnitude of steady state experimental currents was found to be slightly higher than the analytical results. Further investigations are required to validate the proposed equivalent circuit models that include harmonics for estimating current responses of the motor. This will be a subject matter of another paper.

V. CONCLUSIONS

This paper presents basic equivalent circuit models that can be used for dynamic performance analysis of a hysteresis IPM motor drive for submersible pump loads. The proposed analytical model can predict speed transients of the motor with reasonably good accuracy. However, due to experimental limitations, the proposed model is not fully validated for other motor states such as currents, electro-magnetic torque, etc. Further analytical and experimental studies need to be carried out for exact modeling including harmonics of a hysteresis IPM motor.

APPENDIX

TABLE I: DESIGN PARAMETERS OF THE HYSTERESIS IPM MOTOR

Symbol	Name	Value
r_{in}	stator inner diameter	151 mm
r_{out}	stator outer diameter	250 mm
N_s	number of turns/coil	27
N_c	number of coils	48
μ/μ_0	relative permeability elliptic loop	18
r_r	rotor outer diameter	150 mm
l	length of the rotor ring	105 mm
t_r	thickness of the ring	16 mm
l_g	length of the airgap	0.5 mm
t_m	thickness of the PM	6.25 mm
w	width of the PM	40 mm
γ	angular width PM	38 deg.
BH	energy product of 36% Co-Steel	1 MGOe

REFERENCES

[1] O. J. Romero and A. Hupp, “Subsea electrical submersible pump significance in petroleum offshore production, "*ASME J. of Ener. Res. Techn*., vol. 136, no. 1, pp. 012902, Sept. 2014.
[2] T. R. Brinner, R. H. McCoy and T. Kopecky, "Induction versus permanent-magnet motors for electric submersible pump field and laboratory comparisons, " *IEEE Trans. on Ind. Appl.,* vol. 50, no.1, pp. 174-181, Jan. 2014.
[3] H. Hauser, Y. Melikhov and D. C. Jiles, “Examination of the equivalence of ferromagnetic hysteresis models describing the dependence of magnetization on magnetic field and stress”, *IEEE Trans. on Magn*., Vol. 45, No. 4, pp. 1940-1949, April 2009.
[4] M. A. Copeland and G. R. Slemon, “An analysis of the hysteresis motor II-the circumferential-flux machine”, *IEEE Trans. on Power App. Syst.*, vol. 83, no. 6, pp. 619-625, June 1964.
[5] S. Miyairi and T. Kataoka, "A basic equivalent circuit of the hysteresis motor", *IEE Trans. of Japan*, vol. 85, pp. 41-50, Oct. 1965.
[6] R. Qin and M. A. Rahman, “Magnetic equivalent circuit of PM hysteresis synchronous motor”, *IEEE Trans. on Magn*., vol. 39, no. 5, pp. 2998 – 3000, Sept. 2003.
[7] J. J. Nitao et.al., “Equivalent Circuit Modeling of Hysteresis Motors”, Law. Liv. Nat. Lab., Liv., CA, Tech. Rep. LLNL-TR-416493, July 2009.
[8] J. F. Gieras, et. al. , “Calculation of Synchronous Reactances of Small Permanent-Magnet Alternating-Current Motors: Comparison of Analytical Approach and Finite Element Method with Measurements”, *IEEE Trans. on Magn.*., vol. 34, no. 5, pp. 3712-3720, Nov. 1998.
[9] Maxwell Online Help: Release v15.0 (December 2013), ANSYS, Inc., [Online], Available: http: www.ansys.com.